EES Solar

PAPER

View Article Online
View Journal | View Issue

Cite this: *EES Sol.*, 2025, **1**, 378

Circular management of perovskite solar cells using green solvents: from recycling and reuse of critical components to life cycle assessment†

Valentina Larini,[a] Changzeng Ding,[b] Bingzheng Wang,[c] Riccardo Pallotta,[a] Fabiola Faini,[a] Lorenzo Pancini,[a] Zhenhua Zhao,[b] Silvia Cavalli,[a] Matteo Degani,[a] Michele De Bastiani,[a] Filippo Doria,[a] Chang-Qi Ma,[b] Fengqi You[cde] and Giulia Grancini*[a]

Received 13th September 2024
Accepted 26th April 2025

DOI: 10.1039/d4el00004h

rsc.li/EESSolar

Environmental needs and international regulations urgently ask for a robust practice for the recycling and reusing of critical components of perovskite solar cells (PSCs) to reduce the primary material demand and energy consumption. This work demonstrates a circular approach based on green solvents to refurbish critical materials of PSCs, *i.e.* SnO_2-coated indium tin oxide substrates, PbI_2 and Spiro-OMeTAD. Using such recovered materials (and purifying the employed solvents) we fabricate PSCs in an iterative way keeping 98.4% of the initial average efficiency. This comes from an efficient re-utilization of single components, as rationalized by investigating interfaces and device properties upon each recycling step. Concomitantly, we compare the proposed recovery strategy with the conventional landfill treatment for PSCs and silicon photovoltaics through a comparative life cycle assessment (LCA). LCA results reveal that the recovery scenario is preferable to landfilling in reducing energy requirements and environmental footprint.

Broader context

With more than 90% of the global economy still being linear, we almost exclusively rely on new, virgin raw materials (including minerals, ores, biomass and fossil fuels). Therefore, shifting our mindset towards circularity is crucial, especially at the design stage of new products. In this work we propose a recovery method to reuse and recycle critical materials from perovskite solar cells (PSCs), new photovoltaic technologies now entering the market. Materials are refurbished employing green solvents and utilised to fabricate recovered PSCs. To close the loop, solvents are restored and re-inserted in the recovery process. The developed method results to be more sustainable than the landfill scenario and environmentally advantageous even after its third iteration.

Introduction

Among emerging photovoltaics (PVs), perovskite solar cells (PSCs) stand out as promising candidates to advance towards carbon neutrality by 2050, due to their low energy payback time (in the order of months) and levelized cost of electricity and their outstanding record power conversion efficiency (PCE) of 26.7%.[1–4] The International Energy Agency (IEA) has recently reported that the global manufacturing capacity for solar PVs will likely more than double in the next five years, in alignment with the milestones set to reach Net Zero by 2050.[5] The rapid expansion of photovoltaic (PV) systems has prompted countries across the globe to enforce extended producer responsibility (EPR) on PV manufacturers, requiring them to take responsibility for the collection and recycling of their PV product waste. This is reflected in regulations such as the WEEE Directive 2012/19/EU in the European Union, as well as similar legislation in Asia and the United States. Indeed, the International Renewable Energy Agency stated that 60 Mt of solar PV waste will be generated worldwide by 2025,[6] while other studies predicted scenarios considering between 50 (best-case) and 160 (worst-case) million metric tons of PV module waste.[6] Although these numbers are much smaller compared to the waste generated by other sources of energy (*i.e.* coal ash and oil),[6] conceiving end-of-life strategies for deployed PV panels becomes crucial to limiting their dependence on virgin raw materials and lowering

[a]*Department of Chemistry, INSTM, University of Pavia, Via T. Taramelli 14, 27100 Pavia, Italy. E-mail: giulia.grancini@unipv.it*

[b]*Innovation Laboratory & Printable Electronics Research Center, Suzhou Institute of Nano-Tech and Nano-Bionics (SINANO), Chinese Academy of Sciences (CAS), Ruoshui Road 398, Suzhou, 215123, China*

[c]*Systems Engineering, College of Engineering, Cornell University, Ithaca, NY 14853, USA*

[d]*Robert Frederick Smith School of Chemical and Biomolecular Engineering, Cornell University, Ithaca, NY 14853, USA*

[e]*Cornell Atkinson Center for Sustainability, Cornell University, Ithaca, NY 14853, USA*

† Electronic supplementary information (ESI) available. See DOI: https://doi.org/10.1039/d4el00004h

energy consumption.[7] PSC manufacturers recently started to advertise their first commercial products and the PSC market size is forecasted to steadily grow in next years.[8,9] Moreover, since environmental impacts of up to 80% of products are determined at the design phase, foreseeing an end-of-life strategy for PSCs is likewise fundamental.[10] With material management accounting for two-thirds of global greenhouse gas emissions, a circular economy approach should be considered.[11] Indeed, the reduction of primary material consumption is a key aspect for environmental, economic, and social sustainability. It is directly linked to natural resource conservation, environmental impacts, climate change, and economic efficiency. Additionally, stricter regulations and the demand for responsible business practices encourage companies to reduce primary resource use.[12–16] The scarcity of some finite resources makes this transition even more urgent. Circular economy is a model of production and consumption that aims to reduce waste to a minimum and, once a product reaches its end of life, to create further value by recycling the contained materials and keeping them within the economy.[17]

Several studies have been conducted to recover critical components of PSCs, such as transparent conductive oxide (TCO)-coated substrates[18–23] and toxic lead iodide (PbI_2).[24–29] Efforts have also been made to simultaneously recover those and other critical components of PSCs.[30] Many published studies, however, employ harmful and toxic solvents to collect and recover the various components of PSCs. Indeed, although achieving comparable or even higher PCEs for recycled devices with respect to fresh devices, several studies employ *N*,*N*-dimethyl formamide (DMF) to dissolve the perovskite layer.[31–33] DMF is a fetotoxic solvent, it is harmful if inhaled and if in contact with skin and it is included in the candidate list of substances of very high concern, as part of the regulation of the European Chemicals Agency.[34] Therefore, its use should be limited if possible. Feng *et al.* used butylamine, due to its suitable boiling point and solubility, to dissolve the perovskite and to recrystallize high purity methylammonium lead iodide ($MAPbI_3$) crystals.[35] However, butylamine is classified with acute toxicity, skin corrosion and flammability hazard statements.[36] On the other hand, Wang *et al.* adopted a greener method to dissolve the perovskite layer, employing methylamine and reusing the obtained "liquefied perovskite", upon addition of acetonitrile, to re-fabricate the active layer.[37] Nevertheless, they used methylamine together with tetrahydrofuran (THF) to create a so-called "bleacher solution" that simultaneously dissolves the hole-transport layer (HTL) and the perovskite layer of the PSC. Although this method enables the selective collection of all components of the PSC in one single step, the use of THF is not as convenient, since THF is a suspected carcinogenic substance.[38,39] Hence, a process that simultaneously recovers all critical components of PSCs using safe and environmentally friendly solvents is still lacking.

Herein, we propose a multistep process that enables the recovery of several critical components of PSCs, such as the tin oxide (SnO_2)-coated indium tin oxide (ITO) substrates, the toxic PbI_2 and the expensive $N^2,N^2,N^{2\prime},N^{2\prime},N^7,N^7,N^{7\prime},N^{7\prime}$-octakis(4-methoxyphenyl)-9,9′-spirobi[9*H*-fluorene]-2,2′,7,7′-tetramine (Spiro-OMeTAD), with the use of green and safe solvents, *i.e.* deionized water (DI H_2O), ethanol (EtOH) and ethyl acetate (EtOAc),[40,41] which are purified by distillation to be inserted in the recovery loop. Although Spiro-OMeTAD may not be the best candidate for achieving high long-term stability in devices, we believe that, due to the similar chemical properties of the HTL used, our method could be applied to other HTL compositions. To test the efficacy of our method, we fabricated PSCs employing fresh and recovered materials and compared their PV performances. Moreover, to understand the contribution of each recovered component to the recycled device performance, we studied single-component recovery processes and compared the optical, electronic, morphological and compositional properties of fresh and recovered materials. Furthermore, we assessed through a life cycle assessment (LCA) the environmental footprint reduction and energy return benefits of our recovery process in comparison to those obtained by the same type of analysis for both landfill treatment of PSCs and silicon PVs. This evaluation was performed considering various possible module lifetimes and recovery iterations.

Experimental

Materials

Acetone (≥99.8%), 2-propanol (IPA, ≥99.8%), ethanol (EtOH, absolute, ≥99.8%), ethyl acetate (EtOAc, ≥99.5%), $N^2,N^2,N^{2\prime},N^{2\prime},N^7,N^7,N^{7\prime},N^{7\prime}$-octakis(4-methoxyphenyl)-9,9′-spirobi[9*H*-fluorene]-2,2′,7,7′-tetramine (Spiro-OMeTAD, 99%), bis(trifluoromethane)sulfonimide lithium salt (Li(TFSI), 99.95%), acetonitrile (ACN, anhydrous, 99.8%), and 4-*tert*-butylpyridine (4-tBP, 98%) were purchased from Sigma-Aldrich. Hellmanex III cleaning concentrate was purchased from Hellma. Tin(IV) oxide (SnO_2, 15% in H_2O) was purchased from Alfa Aesar. Lead iodide (PbI_2, >98.0%) was purchased from TCI. Formamidinium iodide (FAI, >99.99%), methylammonium chloride (MACl) and 4-methylphenethylammonium chloride (MePEACl) were purchased from GreatCell Solar Materials. Chlorobenzene (CB, extra dry, 99.8%), dimethyl sulfoxide (DMSO, ≥99.9% Extra Dry), and *N*,*N*-dimethylformamide (DMF, 99.8%, Extra Dry) were purchased from Acros Organics.

Device fabrication

ITO-coated glass substrates were cleaned in acetone and IPA by sonicating for 15 minutes in each solvent. Substrates were then dried with a N_2 airflow and subjected to oxygen-plasma treatment for 10 minutes. SnO_2 colloidal dispersion was diluted to 10 wt% in water, spin-coated onto ITO/glass substrates and annealed at 150 °C for 30 minutes. Subsequently, SnO_2-coated substrates were UV-ozone treated for 30 minutes. To prepare the perovskite precursor solution (1.2 M), PbI_2, FAI and MACl (35 mol%) were dissolved in DMF : DMSO = 4 : 1, with 5 mol% PbI_2 excess. The precursor solution was spin-coated onto SnO_2-coated substrates, 150 μL of chlorobenzene was dropped 10 seconds after the beginning of the spin-coating process for the antisolvent procedure and the substrates were annealed at 150 °C for 30 minutes. Subsequently, the $FAPbI_3$ perovskite layer was

passivated with a MePEACl solution 0.01 M in IPA.[42] To fabricate the hole-transport layer, Spiro-OMeTAD was dissolved in CB (80 mg mL^{-1}) and 17.5 μL of Li(TFSI) (500 mg mL^{-1} in ACN) and 28.8 μL of 4-tBP were added to 1 mL of solution. The doped solution was spin-coated onto the perovskite layer. Finally, 80 nm of Au was thermally evaporated on the device, producing devices of 0.045 cm^2 active area as a result of the overlapping area between the ITO and the metal contact.

Devices and solvent recovery

ITO/SnO_2 substrates were recovered from end-of-life PSCs, while PbI_2 and Spiro-OMeTAD were recycled from standard devices fabricated with either the drop-cast perovskite or drop-cast hole transport layer (HTL), depending on the layer that is intended to be recycled. The fabrication of drop-cast layers that provide similar material quantities to large-area modules is necessary because of the small area of lab-scale PSCs, which yields only hundreds of nanograms of perovskite material and HTL, preventing any recovery attempt. Devices were dipped in EtOAc to dissolve the Spiro-OMeTAD layer and induce Au delamination. Au flakes were collected by filtration while Spiro-OMeTAD was purified from Li(TFSI) and 4-tBP dopants by extraction with MilliQ H_2O. Purified Spiro-OMeTAD powder was collected by rotary evaporation. Subsequently, substrates were dipped into DI H_2O and sonicated for 10 minutes to dissolve the perovskite layer. PbI_2 was precipitated by EtOH addition and re-collected by centrifugation. PbI_2 powder was purified by re-dispersion with EtOH, followed by centrifugation, for four times and then evaporated under reduced pressure and dried at 80 °C for 4 hours. The obtained ITO/SnO_2 substrates were further cleaned by sonication in cleaning solution for 10 minutes, DI H_2O for 10 minutes, acetone for 15 minutes and IPA for 15 minutes. Substrates were then dried with a N_2 flow and subjected to UV-ozone treatment for 30 minutes prior to reuse. To fabricate recovered devices, restored ITO/SnO_2, recycled PbI_2 and recycled Spiro-OMeTAD were employed either simultaneously or singularly adopting the same procedure used to fabricate fresh PSCs. For multiple recovery iterations, recovered components were subjected to the same recovery procedure multiple times. EtOAc, EtOH and DI H_2O solvents were purified employing a simple distillation apparatus. The recovery yield for each material was calculated with eqn (1) and averaged between three replications:

$$\text{Recovery yield}_{\text{single component}} = \frac{\text{mass of recovered material}}{\text{mass of initial material}} \times 100 \quad (1)$$

Recovery yield for the all-component-recovered devices was calculated as a weighted mean with eqn (2):

$$\text{Recovery yield}_{\text{all components}} = \frac{\sum \left(\text{mass of recovered material} \times \text{recovery yield}_{\text{single component}}\right)}{\sum \text{mass of initial material}} \quad (2)$$

The glass substrate mass was not included in the calculation of the all-component recovery yield since it is not an active layer. Moreover, Au was also excluded from the calculation since its recollection by filtration would yield almost 100% recovery yield but, due to lab-scale fabrication limitations, it could not be re-deposited onto recovered PSCs.

It is worth noting that, since our recycling approach relies on straightforward techniques such as device dipping, solvent filtration, and/or distillation, we are confident that our approach is compatible with industrial-scale processes. Additionally, the design of the recovery protocol for degraded layers is a key aspect in this field, as it simulates realistic operating conditions.[43,44] However, in our work, we decided to focus on the recycling of fresh layers, without considering the evaluation of the recovery process on degraded ones. This decision is motivated by our goal to provide a solid proof of concept for the recycling of all components of the device, even considering multiple iterations.

Current density–voltage characteristics

Current density (J)–voltage (V) measurements were acquired using a Wavelabs SINUS-70″ solar simulator and a Keithley 2400 sourcemeter. The simulated 1 Sun AM1.5G illumination was calibrated using a certified Si reference cell (Open RR-1002, KG5 window). Devices were measured in an ambient atmosphere, at room temperature, in the reverse and forward scan in the 0–1.2 V voltage range at 130 mV s^{-1} scan rate. During measurement, a metal shadow mask with an aperture area of 0.03 cm^2 was used.

Incident photon-to-current efficiency

IPCE measurements were performed with a Cicci Research Arkeo steady-state test module. The wavelength scan range was set between 300 and 900 nm with a scan step of 10 nm.

Scanning electron microscopy

SEM analyses were carried out using a Zeiss EVO MA10 (Carl Zeiss, Oberkochen, Germany). SEM images were recorded with a SEM (Regulus8230) under 5 kV electron beam acceleration voltage.

Time-of-flight secondary ion mass spectroscopy

ToF-SIMS surface and bulk analyses were performed with a TOF-SIMS 5–100, with the pulsed primary ions from a Cs^+ (2 keV) ion gun for sputtering and a Bi^+ ion beam (30 keV) for analysis.

Time-resolved photoluminescence

TRPL curves were collected using a customised optical setup in which the excitation was provided by a pulsed/CW laser at 470 nm (PicoQuant) with a spot diameter of ≈30 μm. The luminescence was analysed with an interferometer (GEMINI by Nireos) and recorded with a single photon detector (IDQuantique) coupled with a Time Tagger (Swabian Instrument). The

scan was performed in pulsed mode (repetition rate of 5 MHz) using an energy fluence of 0.2 μJ cm^{-2}.

Decay curves were fitted with a bi-exponential fit function, reported in eqn (3):

$$y(t) = A_1\, e^{-\frac{t}{\tau_1}} + A_2\, e^{-\frac{t}{\tau_2}} \quad (3)$$

where τ_1 and τ_2 are the lifetimes of two different decay channels for photogenerated charge carriers and A_1 and A_2 are the relative amplitudes.

Transient photocurrent and transient photovoltage

TPV and TPC analyses were performed with a commercial apparatus (Arkeo, Cicci Research s.r.l.) based on a high-speed Waveform Generator that drives a high-speed LED (5000 kelvin). The device is connected to a transimpedance amplifier and a differential voltage amplifier to monitor short circuit current or open circuit voltage. Measurements were conducted under 1 Sun illumination and constant bias was perturbed with short light pulses of 200 μs width.

Decay curves were fitted with a mono-exponential fit function, reported in eqn (4):

$$y(t) = A\, e^{-\frac{t}{\tau}} \quad (4)$$

where τ is the lifetime and A is the amplitude.

X-ray photoelectron spectroscopy

XPS analysis was conducted with a PHI 5000 VersaprobeII system coupled with an Al X-ray source. X-ray beam voltage was set to 15 kV.

Atomic force microscopy

AFM images were acquired with a TriA-SPM microscope (A.P.E. Research S.r.l., Trieste, Italy) in non-contact mode, using NSC15/AI BS probes (Mikromasch – Innovative Solutions Bulgaria Ltd) and scanning areas of 5 × 5 μm and 10 × 10 μm. AFM images were edited with Gwyddion[36] and root mean square roughness (R_q) data were processed with the specific software function.

UV-vis spectroscopy

UV-Vis spectroscopy measurements were performed employing a PerkinElmer LAMBDA 1050+ UV/Vis/NIR spectrophotometer. To generate the calibration line, measurements were replicated three times for each concentration and all acquisitions were repeated three times.

X-ray diffraction

XRD patterns were acquired using a Bruker D2 X-ray diffractometer coupled with a Cu X-ray tube ($\lambda = 1.5418$, 300 W, 30 kV) and a Lynxeye (1D mode) detector. Measurements were performed adopting 0.02° step size and 1 step per s scan rate.

Proton nuclear magnetic resonance spectroscopy

^{1}H-NMR spectra were recorded on a Bruker Advance 400 MHz.

Fluorometric analysis

Fluorometric analysis for solvent contamination assessment was conducted employing a fluorometric Pb detection system, based on the Pb-selective BODIPY fluorophore that emits when the analyte – Pb in this case – is detected.[45] Fluorescence spectra were recorded with an Agilent Cary Eclipse spectrofluorometer, at a scan rate of 600 nm min^{-1}, in the 495–600 nm interval, manual voltage 550 V, with bandwidth of excitation and emission slits at 5 nm. Measurements were replicated three times for each sample and all acquisitions were repeated three times.

Statistical analysis

OriginPro 2018 software was employed to perform statistical analysis. For photovoltaic parameters and TRPL lifetime and amplitude values, dataset was arranged in box charts, where whiskers limit the 1.5 interquartile range, the box identifies the 25th and 75th percentiles and the horizontal line represents the average value. Sample size (n) is reported for each analysis. For TRPL lifetime and amplitude values, average values with error bars are also reported.

Life cycle assessment modelling

In conducting our LCA, we have evaluated a variety of environmental impacts utilizing the PEF methodology.[46,47] Our analysis uses one square meter of PSC module area as the functional unit.[48] However, it does not imply the actual size of the commercial solar panels.[49,50] Previous LCA studies on PSCs have shown that even minimal usage of precious metals in electrodes can significantly impact most environmental categories.[51,52] As a result, using costly electrode materials, like gold and silver, may not be sustainable for large-scale PSC production. Therefore, we use non-precious transition metals, particularly copper, as potential replacements for noble metals in manufacturing PSCs.[53]

We developed a comprehensive life cycle inventory (LCI) dataset detailing material and energy flows at each life cycle stage for the studied perovskite solar cell. This dataset material and energy utilization calculations draw upon experimental data from cell production and recycling stages. We converted all energy forms into their electrical equivalents, which is in line with standard practices found in the literature.[51] Moreover, for processes expected to be upscaled to industrial levels, our energy and material consumption evaluations are based on extrapolations from the existing literature.[54]

We organized the results using various impact metrics in the life cycle impact assessment (LCIA) phase. The LCIA data for the perovskite solar cell provided valuable insights into how the materials used and the processes involved contribute to different environmental impact indicators. The sustainability metrics were analysed considering several recycling iterations and specific PSC lifetimes. These analyses allowed us to make data-driven recommendations for enhancing the proposed recycling method sustainable deployment and periodic maintenance.

Results and discussion

Recovery protocol

To design our recovery method, we followed the waste hierarchy reported in the EU directive 2008/98/EC, which defines the order of actions that should be taken to manage waste.[55] The hierarchy, from most to least preferred, goes through prevention, reuse, recycling, other recovery and disposal.[55] Therefore, where possible, we reused components instead of recycling raw materials. More specifically, we define the reuse of ETL-coated TCO substrates as "restoration" since the process involves some steps to return to their initial condition. The word "recovery" will be used hereafter to identify processes that involve both recycling and restoration. Moreover, we employed the CHEM21 solvent guide, which combines safety, health and environmental criteria with LCA considerations, to select the safest and most environmentally friendly solvents.[41]

Fig. 1(a) presents a schematic illustration of the process adopted to recycle and restore, by selective dissolution, different layers of nip PSCs, whose architecture is reported in the scheme. All recovered components were used to re-fabricate PSCs and the employed solvents were purified by distillation. In order to test the efficacy of our recovery method, we compared the PV performances of PSCs fabricated with recovered and fresh materials and investigated the properties of the obtained materials. Fig. 1(b) displays the recycling yield for single-component and all-component recovery processes, calculated as percentage of mass recovered. The recovery yields for all-component-recovered devices are close to 100% for ITO/SnO_2, 99.1 ± 0.3% for PbI_2 and 89 ± 4% Spiro-OMeTAD, ultimately leading to a weighted mean of 81 ± 2% for the full recovery stack. Moreover, Fig. 1(b) summarizes the PV parameter percentage loss for recovered PSCs with respect to fresh PSCs, in the case of both single-component and all-component recovery processes. Note that Fig. S23–29† report the PV parameter distribution of devices fabricated with the non-optimized recovery procedure. While PbI_2 recycling does not induce significant PV performance variation, ITO/SnO_2 restoration mainly impacts the average short-circuit current density (J_{SC}) and the average fill factor (FF), which are reduced by 3.0% and enhanced by 3.6%, respectively. Likewise, Spiro-OMeTAD recycling produces a great enhancement of the average FF (increasing it by 5.5%). These results are reflected in the performance of the all-component-recovered devices, where a great enhancement in the average FF (increase of 7.5%) compensates for an open-circuit voltage (V_{OC}) and J_{SC} decrease (decrease of 3.9% and 4.8%, respectively). The PCE, V_{OC}, J_{SC}, FF and hysteresis index (HI) statistical analyses for fresh and all-component-recovered PSCs are reported in Fig. 1(c) and S1 (ESI).† For PSCs fabricated by simultaneously employing all recovered components, there is a 98.4% PCE retention with respect to fresh PSCs, which is a demonstration of the effectiveness of our recovery method. Incident photon-to-current efficiency (IPCE) and integrated current density curves for fresh and recovered devices are presented in Fig. S2 (ESI).† In order to further investigate the properties of the recovered devices, we acquired scanning electron microscopy (SEM) cross-sectional images and performed time-of-flight secondary ion mass spectroscopy (ToF-SIMS) analysis, whose results are presented in Fig. 1(d). Spiro-OMeTAD and ITO/SnO_2 layers display comparable morphology to fresh ones, while the formamidinium lead iodide ($FAPbI_3$) perovskite layer fabricated with recycled PbI_2 presents more grain boundaries than the $FAPbI_3$ fabricated with fresh PbI_2, whose implications will be further investigated later on in the paper. ToF-SIMS analysis, superimposed to SEM images, for Au, C, PbI_2 and In does not show any relevant difference between fresh and recovered devices, again confirming the efficacy of our protocol. Furthermore, we tested the effect of multiple recovery iterations on the PV performance of our PSCs. Results are presented in Fig. S3 (ESI),† where V_{OC}, J_{SC}, FF and PCE box charts are provided for fresh devices as well as for the first, second and third recovery iterations. When going from fresh materials to third-time recovered components, 84.2% of the original average PCE is maintained. While J_{SC} remains almost constant from the first to the third recovery iteration, V_{OC} and FF progressively decrease. On one hand, the V_{OC} trend can be correlated with the progressive V_{OC} reduction displayed by PSCs fabricated with multiple times restored ITO/SnO_2 substrates (see Fig. S4, ESI†). On the other hand, the FF reduction trend cannot be ascribed to one single material recovery process, but it results from a convolution of several effects that multiple recovery iterations have on PSC performance. Despite the iteration of the recovery process resulting in a decline in the PV parameters, we believe that, with continuous advancements in the lifetime of state-of-the-art perovskite solar cells—at least reaching a level comparable to that of silicon-based technologies—and its relative mass scale production, our recovery protocol could ensure the use of the same materials for over half a century. Indeed, Fig. S3† shows a negligible decrease in the PV parameters after one recovery cycle, and a decrease of around 10% after the second cycle.

Single-component recovery

To understand each single-component contribution to the all-component-recovered devices, we fabricated PSCs employing either restored ITO/SnO_2, recycled PbI_2 or recycled Spiro-OMeTAD. Fig. 2(a) displays the V_{OC}, J_{SC}, FF and PCE box charts of PSCs fabricated with fresh and restored ITO/SnO_2. While V_{OC} and J_{SC} decrease upon the restoration process, FF is widely increased, leading to the same average PCE for fresh and restored samples. To study the recombination processes occurring at the SnO_2/perovskite interface, we fabricated full stack devices with fresh and restored ITO/SnO_2, without metal contact deposition, and performed time-resolved photoluminescence (TRPL) analysis (Fig. 2(b)). The measurement was conducted on a statistic of 5 samples and box chart results and average values with error bars for photogenerated charge carrier lifetimes (τ_1 and τ_2) and amplitudes (A_1 and A_2) are presented in Fig. S6 (ESI).† Both τ_1 and τ_2 are statistically higher for fresh samples, being reduced by 24% and 31%, respectively, upon the restoration process. τ_1 reduction can be ascribed to faster

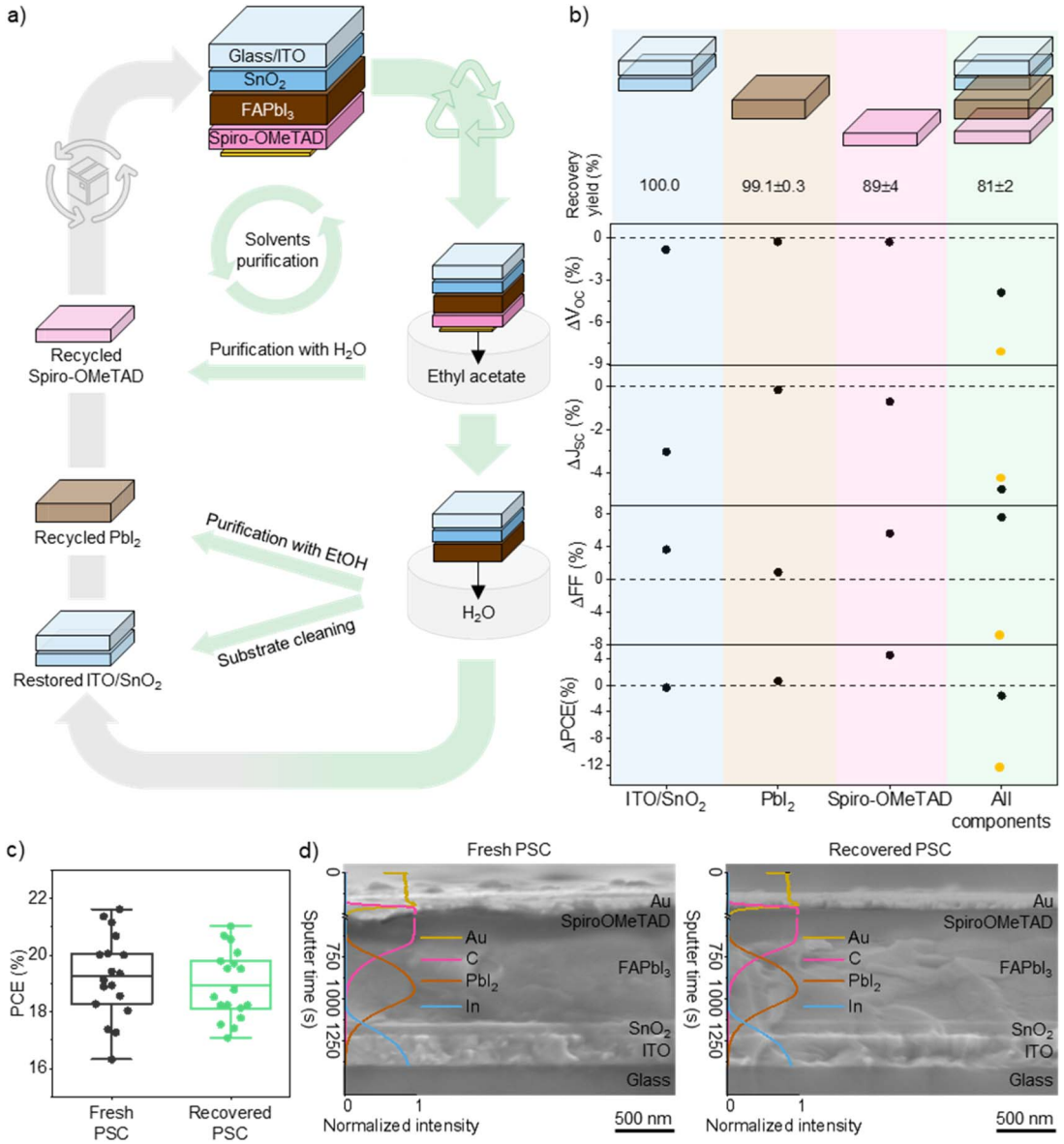

Fig. 1 (a) Schematic illustration of the recovery processes for three critical components of PSCs, *i.e.* SnO_2-coated ITO substrates, PbI_2 and Spiro-OMeTAD. Recycling/restoration processes are identified by green arrows, while re-fabrication processes are identified by gray arrows. (b) Photovoltaic parameters percentage variation of recovered samples with respect to fresh samples for single-component and all-component recycling/restoration processes. Recycling yield, calculated as percentage of mass recovered, is reported for single-component and all-component recycling/restoration processes. Yellow dots highlight the variation of PV parameters after the third recovery cycle of all components. (c) Power conversion efficiency box chart for PSCs fabricated with fresh components ("Fresh PSC") and restored ITO/SnO_2, recycled PbI_2 and Spiro-OMeTAD, simultaneously ("Recovered PSC"). Sample size is 18. Whiskers limit the 1.5 interquartile range, the box identifies the 25th and 75th percentile and the horizontal line represents the average value. (d) SEM cross-sectional images of PSCs fabricated by employing fresh components and, simultaneously, restored ITO/SnO_2 and recycled PbI_2 and Spiro-OMeTAD. ToF-SIMS curves for Au, C, PbI_2 and In are superimposed on SEM images.

charge extraction at the SnO_2/perovskite interface, which is reflected in the average FF increase.[56] On the other hand, τ_2 decrease can be related to higher bulk recombination, which negatively affects the V_{OC}.[57] To further confirm these results, we performed transient photocurrent (TPC) and transient photovoltage (TPV) measurements, reported in Fig. 2(c) and S7 (ESI),† respectively. For both TPC and TPV curves, lifetime (τ) was lower in the case of PSCs fabricated with restored ITO/SnO_2 substrates ($\tau_{TPC\text{-}fresh} = 1.13$ μs, $\tau_{TPC\text{-}restored} = 0.96$ μs, $\tau_{TPV\text{-}fresh} = 2.80$ μs, $\tau_{TPV\text{-}restored} = 1.51$ μs), corroborating the faster charge extraction and higher charge carrier recombination assumptions.[58,59] In order to correlate the photoelectronic properties of fresh and restored samples with morphological and compositional aspects, we conducted ToF-SIMS analysis on fresh and restored ITO/SnO_2 substrates. Surface maps, reported in Fig. 2(d), display a reduction in the K^+ signal intensity and an increase in

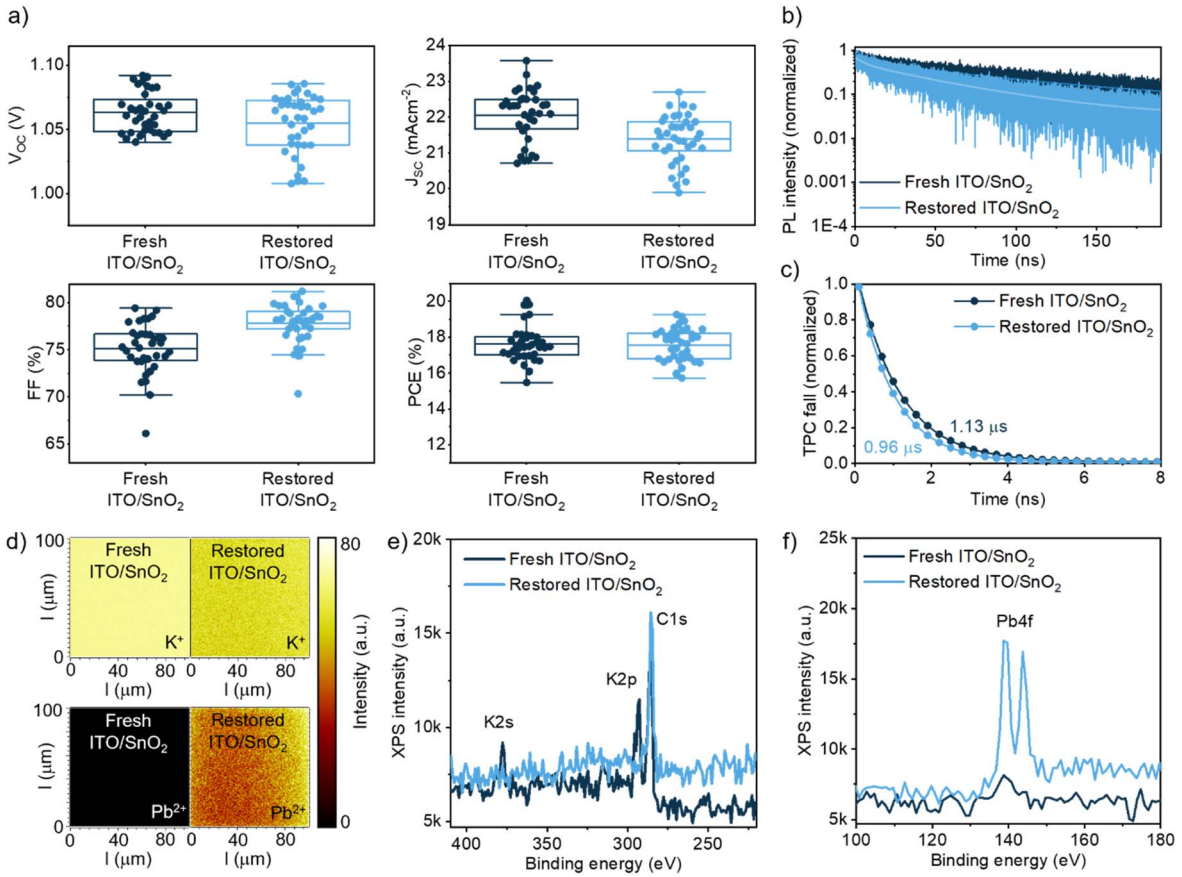

Fig. 2 (a) Photovoltaic parameter box charts for PSCs fabricated with fresh and restored ITO/SnO_2 substrates. Sample size is 38. Whiskers limit the 1.5 interquartile range, the box identifies the 25th and 75th percentile and the horizontal line represents the average value. (b) TRPL decay of full-stack devices – without Au metal contact – fabricated with fresh and restored ITO/SnO_2 substrates. (c) TPC decay of PSCs fabricated with fresh and restored ITO/SnO_2 substrates. Carrier lifetime values are reported for each curve. (d) ToF-SIMS surface maps of fresh and restored ITO/SnO_2 substrates for K^+ and Pb^{2+} ions. (e and f) XPS of fresh and restored ITO/SnO_2 substrates in the characteristic binding energy range of K 2s, K 2p and Pb 4f signals.

the Pb^{2+} signal intensity upon restoration. These results are further confirmed by X-ray photoelectron spectroscopy (XPS) measurements, presented in Fig. 2(e), (f) and S8 (ESI),† where K 2s and K 2p peaks disappear and Pb 4f peaks arise after ITO/SnO_2 restoration. The K^+-based species on the surface of the SnO_2 ETL are ascribable to potassium hydroxide (KOH), which is inserted into the SnO_2 precursor solution by the supplier.[60] Since it is reported that KOH passivates the SnO_2/perovskite interface, suppressing non-radiative recombination, its partial removal upon substrates restoration would increase interfacial recombination, negatively impacting the average V_{OC} of the devices.[60] Moreover, Abdi-Jalebi *et al.* found that potassium salt passivation would not only increase the V_{OC} but also the J_{SC} of their devices, due to increased carrier mobility, which could be the reason behind the higher J_{SC} displayed by PSCs fabricated with fresh substrates with respect to restored ITO/SnO_2.[61] On the other hand, Pb^{2+} species, ascribed to PbI_2 from ToF-SIMS measurements (see Fig. S9, ESI†), seem to have an impact on charge extraction. Indeed, it is reported that, having a wider bandgap than the perovskite, PbI_2 can act as a hole sink.[62] In particular, holes generated in the ETL preferentially recombine with electrons formed in PbI_2, facilitating the extraction at the n-contact of electrons generated in the perovskite, thus improving the average FF.[63,64]

To study the effect of PbI_2 recycling on the properties of the active layer, we fabricated $FAPbI_3$ thin films employing fresh and recycled PbI_2. SEM images, displayed in Fig. 3(a), demonstrate that recycled PbI_2 induces the formation of smaller perovskite grains. Moreover, R_q values extracted from atomic force microscopy (AFM) images, shown in Fig. S10 (ESI),† indicate that $FAPbI_3$ fabricated with recycled PbI_2 has higher R_q (of 3.2 nm) than the fresh sample (R_q = 2.6 nm). Although UV-Vis absorbance measurement and Tauc plot analysis as well as XRD and XPS measurements show no difference between $FAPbI_3$ and PbI_2 thin films before and after recycling (Fig. S11 and S12, ESI†), the different crystallization of the perovskite upon PbI_2 recycling impacts the charge carrier lifetime, as demonstrated by TRPL decays (Fig. 3(b) and S13, ESI†). Similarly to the ITO/SnO_2 restoration case, τ_1 and τ_2 both decrease when recycled PbI_2 is used to fabricate the perovskite layer. While τ_1 reduction upon recycling can be ascribed to enhanced charge extraction, τ_2 decrease can be associated with higher

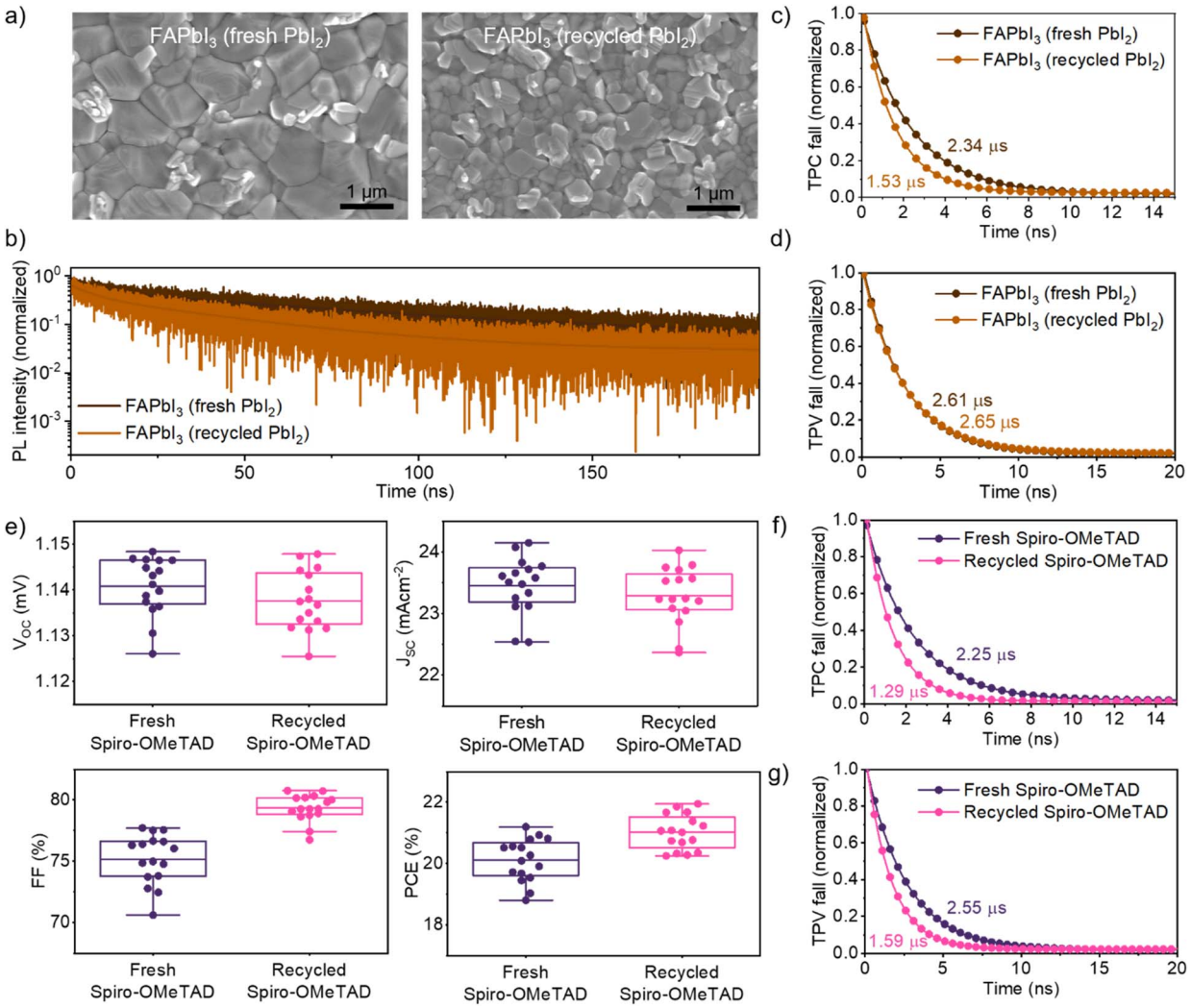

Fig. 3 (a) SEM images of $FAPbI_3$ perovskite fabricated with fresh and recycled PbI_2. (b) TRPL decay of full-stack devices – without Au metal contact – fabricated with fresh and recycled PbI_2. (c) TPC decay of PSCs fabricated with fresh and recycled PbI_2. Carrier lifetime values are reported for each curve. (d) TPV decay of PSCs fabricated with fresh and recycled PbI_2. Carrier lifetime values are reported for each curve. (e) Photovoltaic parameter box charts for PSCs fabricated with fresh and recycled Spiro-OMeTAD. Sample size is 16. Whiskers limit the 1.5 inter-quartile range, the box identifies the 25th and 75th percentile and the horizontal line represents the average value. (f) TPC decay of PSCs fabricated with fresh and recycled Spiro-OMeTAD. Carrier lifetime values are reported for each curve. (g) TPV decay of PSCs fabricated with fresh and recycled Spiro-OMeTAD. Carrier lifetime values are reported for each curve.

non-radiative recombination occurring in the perovskite bulk, as a consequence of the higher amount of grain boundaries. Interestingly, the amplitude A_1, referred to the first decay channel, is enhanced from 26.3 ± 0.9% to 44 ± 4% for $FAPbI_3$ fabricated with fresh and recycled PbI_2, respectively, suggesting that charge extraction becomes almost as significant as bulk recombination. This can possibly explain the absence of variation in the PV parameters displayed by PSCs fabricated with fresh and recycled PbI_2, whose statistical analysis is reported in the box charts of Fig. S14 (ESI).† We speculate that higher bulk recombination is compensated by a better perovskite/charge transporting material (CTM) interface, produced by the smaller grain dimension.[65] This is corroborated by TPC and TPV curves, presented in Fig. 3(c) and (d). Indeed, the faster TPC decay and almost identical TPV lifetimes of devices fabricated with fresh and recycled PbI_2 suggest faster charge extraction and similar charge carrier recombination within the device.

Finally, we assessed the efficacy of our method for Spiro-OMeTAD recycling. Proton nuclear magnetic resonance (^{1}H-NMR) spectroscopy reveals a perfect match between the NMR signals of fresh and recycled Spiro-OMeTAD (see Fig. S15, ESI†), suggesting that the recycled material does not deteriorate with respect to the pristine material. Moreover, fresh and recycled Spiro-OMeTAD exhibit similar morphology, as demonstrated by SEM and AFM images and by R_q analysis, provided in Fig. S16 and S17 (ESI).† Fig. 3(e) presents the V_{OC}, J_{SC}, FF and PCE box charts of PSCs fabricated employing fresh and recycled Spiro-OMeTAD. While V_{OC} and J_{SC} are slightly reduced (by 0.3% and 0.7%, respectively), FF is largely increased by 5.5%, leading to an overall 4.5% average PCE enhancement. Once again, these

results can be rationalized by studying charge carrier extraction and recombination mechanisms. TPC and TPV measurements are reported in Fig. 3(f) and (g), respectively. The shorter TPC carrier lifetime of devices fabricated with recycled Spiro-OMeTAD suggests a faster charge extraction, while the faster TPV decay is ascribable to higher charge carrier recombination occurring in the device with recycled Spiro-OMeTAD.

Interestingly, recycled Spiro-OMeTAD thin films exhibit higher oxidation capacity than fresh ones, as demonstrated by the UV-Vis absorbance spectra in Fig. S18 (ESI).† After 6 days in an oxidizing atmosphere, peaks at around 510 nm, 700 nm and 1480 nm start rising for both samples and they add to the already present 383 nm peak, which is characteristic of neutral Spiro-OMeTAD.[66,67] These additional absorption peaks originate when Spiro-OMeTAD^{2+} and Sprio-OMeTAD^{4+} oxidized forms are created as products of the redox reaction between neutral Spiro-OMeTAD, oxygen and lithium bis(trifluoromethanesulfonyl) imide (Li-TFSI) – which is inserted in the Spiro-OMeTAD precursor solution as the dopant.[67,68] The higher intensity of those peaks for recycled Spiro-OMeTAD suggests a higher oxidation state with respect to the fresh material, which we speculate to arise from the longer exposure of recycled Spiro-OMeTAD to oxygen and Li-TFSI – both prior and after recycling. A higher oxidation state of Spiro-OMeTAD is known to improve the HTL conductivity that results in higher average FF.[68]

Solvent purification

In order to close the recovery loop and further reduce the eco-toxicity of the proposed method,[69] we decided to distil the solvents used for recovering ITO/SnO_2, PbI_2 and Spiro-OMeTAD to re-insert them in the circular process.

To verify the purity of the recovered solvents, we tested the presence of specific contaminants, *i.e.* PbI_2 for DI H_2O and EtOH and Spiro-OMeTAD for EtOAc. To assess the presence of PbI_2 contaminants inside recovered DI H_2O and EtOH, we employed a fluorometric Pb detection system.[43] Fluorescence spectra, reported in Fig. S19 (ESI),† are the most representative curves for the blank solution, distilled solvent and solvent collected from PbI_2 recycling. Three curves were acquired for each sample and each measurement was repeated three times.

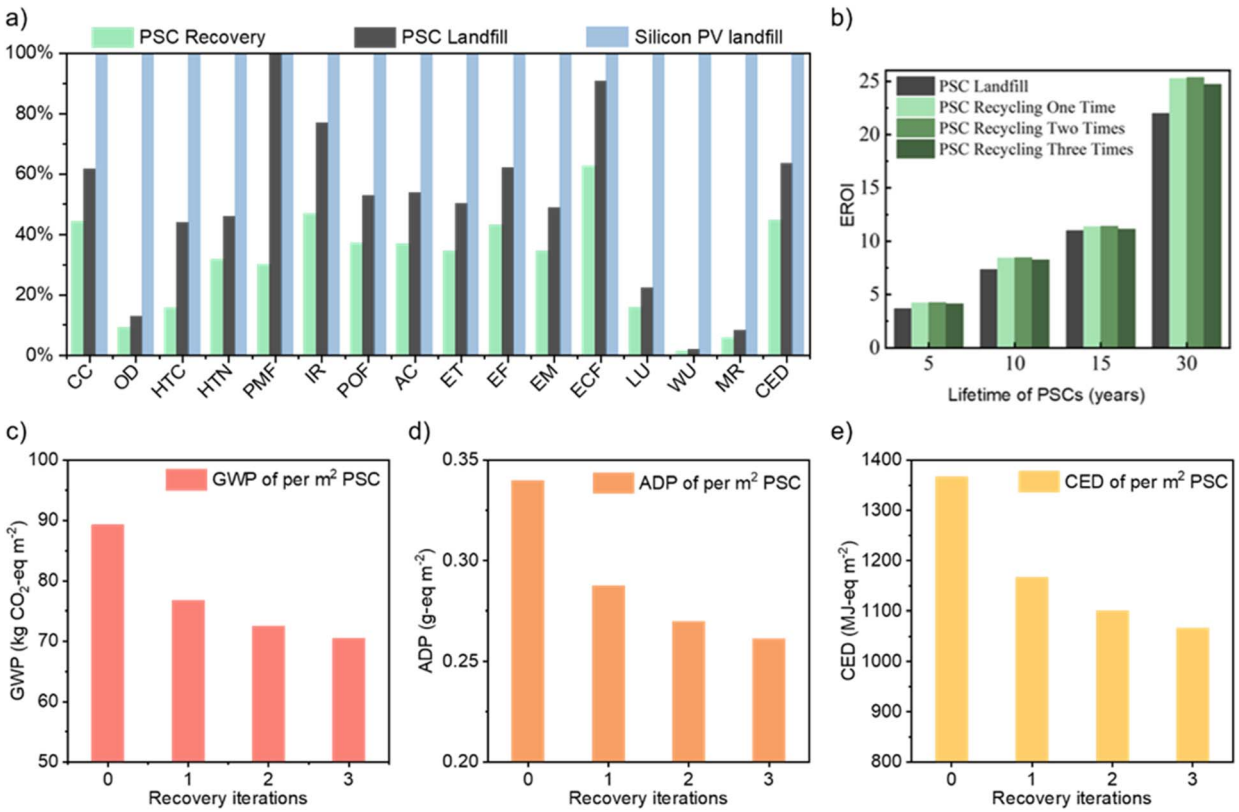

Fig. 4 (a) Comparison of full-spectrum midpoint impact categories between single-crystal silicon PV, PSC recovery, and PSC landfill according to the EF v3.0 method. CC: climate change. OD: ozone depletion; HTC: human toxicity: carcinogenic; HTN: human toxicity: non-carcinogenic; PMF: particulate matter formation; IR: ionizing radiation: human health; POF: photochemical oxidant formation: human health; AC: acidification; ET: eutrophication: terrestrial; EF: eutrophication: freshwater; EM: eutrophication: marine; ECF: ecotoxicity: freshwater; LU: land use; WU: water use; MR: material resources: metals/minerals; CED: cumulative energy demand. (b) Energy Return of Investment (EROI), which is calculated as the ratio of electricity generation to the primary energy invested throughout the life cycle of PVs for the perovskite landfill and perovskite recovery from one to three times under lifetimes of 5, 10, 15 and 30 years. (c) Relative impacts of perovskite multiple recovery in terms of global warming potential (GWP), recovering one time means two square meters PSC fabrication and three times correspond to four square meters. (d) Relative impacts of perovskite multiple recovery in terms of abiotic depletion potential (ADP). (e) Relative impacts of perovskite multiple recovery in terms of CED.

From average data, we calculated that 97.4% and 99.8% of PbI_2 were removed by distillation from DI H_2O and EtOH, respectively. Spiro-OMeTAD removal from EtOAc was, instead, evaluated by UV-Vis absorbance spectroscopy, generating a calibration line on the 383 nm peak. Three curves were acquired for each sample and each measurement was repeated three times. The calibration line and most representative curves for 0.02 M, 0.01 M and 0.001 M concentrations and for distilled EtOAc are reported in Fig. S20 (ESI).† Since the intensity of all curves referred to distilled EtOAc is too close to the photometric accuracy of our spectrophotometer (±0.001 A), we assume that all Spiro-OMeTAD contaminant has been removed from EtOAc.

Life cycle assessment

We conducted a detailed LCA to assess the environmental impacts of the proposed recovery strategy compared to single-crystal silicon PV and PSC landfill disposal methods for waste modules. In this work, the ITO glass, PbI_2 comprising the perovskite layer and Spiro-OMeTAD of PSCs were recovered. The solvents used for recycling were purified. Our evaluation includes both a "cradle-to-cradle" system boundary for our recovery process and a "cradle-to-grave" system boundary for the landfill scenario. For the landfill scenario, detailed in Fig. S21 (ESI),† we considered life cycle stages, including raw material obtainment, PSC fabrication, electricity generation, and eventually landfill. In contrast, our recovery method, shown in Fig. S22 (ESI),† uses a circular approach by recovering the decommissioned PSC devices to reuse crucial components rather than directly landfill them. The stages of raw material collection, PSC fabrication, and electricity production remain consistent in both landfill and recovery scenarios. We assessed midpoint impact categories following the Product Environmental Footprint (PEF) methodology, as outlined in the IEA – Photovoltaic Power Systems Program Task 12 report to reveal the full-spectrum consequences associated with climate change, resource depletion, cumulative energy demand, and so on.[46]

We find that the environmental performance of the proposed recovery method outperforms those of the landfill scenario of traditional silicon PVs in all evaluated indicators (Fig. 4(a)). Specifically, our recovery strategy can significantly reduce the carbon emission associated with PSCs by 55.5% and 28.1% when compared to silicon PV and PSC landfilling, respectively. Besides, compared to PSC landfilling, the recovery strategy can reduce human toxicity by 64.3% (cancer effects) and 31.0% (non-cancer effects). We attribute these merits to our holistic recovery strategy that can restore most components in PSCs, eliminating the need for excessive virgin material inputs. Compared to the landfill scenario, our recovery strategy ultimately yields more electricity per m^2 PSC, even though the process reduces the power conversion efficiency and requires additional energy input. For potential lifetimes of 5, 10, 15 and 30 years the EROI (Fig. 4(b)) values for PSC recovery (one time) are 4.21, 8.42, 11.36 and 24.95 respectively, in contrast to 3.66, 7.33, 11.99 and 22.47 for the landfill scenario. Multiple recovery has the potential to further improve the PSC fabrication energy return through the cyclic utilization of virgin materials. The EROIs when recovering two times are 4.23, 8.45, 11.41 and 25.01. Note that the EROI slightly decreases when recovering three times due to the significant efficiency loss. From the m^2 PSC perspective, multiple recovery can gradually enhance the performance of various indicators (Fig. 4(c) and (e)). For instance, the ADP of PSC gradually decreases from 0.34 to 0.26 g-eq. m^2. It is worth mentioning that longer module lifetimes make market scenarios for many recovery strategies less plausible due to technological advancements occurring during the module lifetime and the emergence of novel materials. In this regard, prior studies have shown that recycling may not be essential if perovskite cells can achieve lifetimes similar to silicon-based systems.[1]

Conclusions

In this work we demonstrated the recovery of several critical components of PCSs, employing green and safe solvents that we purified by distillation. Materials recovery yields reached almost 100.0%, 99.1 ± 0.3% and 89 ± 4% for ITO/SnO_2, PbI_2 and Spiro-OMeTAD, respectively, ultimately leading to an 81 ± 2% overall recovery yield with PSCs displaying 98.4% of the fresh PCE. By fabricating single-component-recovered PSCs, we deconvolved the contribution of each material recovery and correlated V_{OC} and J_{SC} reduction with higher charge carrier recombination and FF enhancement with better charge extraction at the perovskite/CTM interfaces. Moreover, we tested the wider applicability of our recovery protocol by performing multiple recovery iterations that progressively reduced the environmental impact of the device, without critically affecting energy return. With a small amount of additional energy and material inputs, our approach resulted to be favorable with respect to a landfill scenario, as determined *via* LCA. Overall, the developed approach meets the circularity and sustainability requirements set for current technology development, which is crucial for a timely market uptake. We believe that the demonstrated sustainable and practical method can be easily scaled up, reducing the environmental impact of perovskite solar technology and shortening its gap to commercialization.

Data availability

The data that support the findings of this study are available from the corresponding authors upon reasonable request.

Author contributions

Conceptualization: VL, MDB, GG. Methodology: VL, FF, LP, RP, MD, BW. Investigation: VL, CD, ZZ. Formal analysis: VL, CD, BW, FF, SC. Supervision: MDB, FD, CQM, FY, GG. Writing—original draft: VL, BW, FF. Writing—review & editing: VL, FF, SC, FY, GG.

Conflicts of interest

There are no conflicts to declare.

Acknowledgements

The authors acknowledge Edison for the collaboration, the project for infrastructures funded by Regione Lombardia RL3776, the Fondazione Cariplo Economia Circolare 2021 Project "Green flexible hybrid perovskite solar module for the market: from smart lead manipulation to recycling" (FLHYPER, no. 20201067), funded under the "Circular Economy-2020" call, the Ministero dell'Università e della Ricerca (MUR) and the University of Pavia through the program "Dipartimenti di Eccellenza 2023–2027". The LCA work at Cornell University is supported in part by National Science Foundation (NSF) CAREER Award (CBET-1643244). F. Y. acknowledges the partial support from the Eric and Wendy Schmidt AI in Science Post-doctoral Fellowship, a Schmidt Sciences program. The authors are grateful for the technical support from Nano-X vacuum interconnected nanotech workstation of Suzhou Institute of Nano-Tech and Nano-Bionics, Chinese Academy of Sciences (SINANO).

References

1 X. Tian, S. D. Stranks and F. You, Life Cycle Assessment of Recycling Strategies for Perovskite Photovoltaic Modules, *Nat. Sustainability*, 2021, **4**(9), 821–829, DOI: **10.1038/s41893-021-00737-z**.

2 M. De Bastiani, V. Larini, R. Montecucco and G. Grancini, The Levelized Cost of Electricity from Perovskite Photovoltaics, *Energy Environ. Sci.*, 2022, **16**, 421–429, DOI: **10.1039/d2ee03136a**.

3 NREL, Best Research-Cell Efficiency Chart, **https://www.nrel.gov/Pv/Cell-Efficiency**, accessed: April 2023.

4 J. Zhou, L. Tan, Y. Liu, H. Li, X. Liu, M. Li, S. Wang, Y. Zhang, C. Jiang, R. Hua, W. Tress, S. Meloni and C. Yi, Highly Efficient and Stable Perovskite Solar Cells via a Multifunctional Hole Transporting Material, *Joule*, 2024, **8**, 1–16, DOI: **10.1016/j.joule.2024.02.019**.

5 International Energy Agency (IEA), Tracking Clean Energy Progress 2023, 2023.

6 H. Mirletz, H. Hieslmair, S. Ovaitt, T. L. Curtis and T. M. Barnes, Unfounded Concerns about Photovoltaic Module Toxicity and Waste Are Slowing Decarbonization, *Nat. Phys.*, 2023, **19**(10), 1376–1378, DOI: **10.1038/s41567-023-02230-0**.

7 When Circularity Goes from Bad to Worse.

8 Allied Market Research, Perovskite Solar Cell Market Analysis – 2030, **https://www.alliedmarketresearch.com/perovskite-solar-cell-market-A13745**.

9 Precedence Research, Perovskite Solar Cell Market, **https://www.precedenceresearch.com/perovskite-solar-cell-market**.

10 European Commission, A New Circular Economy Action Plan For a Cleaner and More Competitive Europe, 2020.

11 The World Bank, Squaring the Circle- Policies from Europe's Circular Economy Transition, 2022.

12 Reports — IPCC, **https://www.ipcc.ch/reports/**, accessed 2025-04-02.

13 How to Build a Circular Economy, Ellen MacArthur Foundation. **https://www.ellenmacarthurfoundation.org/**, accessed 2025-04-02.

14 UNEP, UN Environment Programme, **https://www.unep.org/**, accessed 2025-04-02.

15 The World Economic Forum. **https://www.weforum.org/**, accessed 2025-04-02.

16 The Organisation for Economic Co-operation and Development, OECD, **https://www.oecd.org/**, accessed 2025-04-02.

17 European Parliament, *Circular Economy: Definition, Importance and Benefits*, 2023, pp. 1–5.

18 X. Feng, S. Wang, Q. Guo, Y. Zhu, J. Xiu, L. Huang, Z. Tang and Z. He, Dialkylamines Driven Two-Step Recovery of NiOx/ITO Substrates for High-Reproducibility Recycling of Perovskite Solar Cells, *J. Phys. Chem. Lett.*, 2021, **12**, 4735–4741, DOI: **10.1021/acs.jpclett.1c00735**.

19 B. Augustine, K. Remes, G. S. Lorite, J. Varghese and T. Fabritius, Recycling Perovskite Solar Cells through Inexpensive Quality Recovery and Reuse of Patterned Indium Tin Oxide and Substrates from Expired Devices by Single Solvent Treatment, *Sol. Energy Mater. Sol. Cells*, 2019, **194**, 74–82, DOI: **10.1016/j.solmat.2019.01.041**.

20 J. M. Kadro, N. Pellet, F. Giordano, A. Ulianov, O. Müntener, J. Maier, M. Grätzel and A. Hagfeldt, Proof-of-Concept for Facile Perovskite Solar Cell Recycling, *Energy Environ. Sci.*, 2016, **9**, 3172–3179, DOI: **10.1039/c6ee02013e**.

21 Z. Ku, X. Xia, H. Shen, N. H. Tiep and H. J. Fan, A Mesoporous Nickel Counter Electrode for Printable and Reusable Perovskite Solar Cells, *Nanoscale*, 2015, **7**, 13363–13368, DOI: **10.1039/c5nr03610k**.

22 X. Tian, B. Roose, S. D. Stranks and F. You, Periodic Module Rejuvenation Provides Early Market Entry for Circular All-Perovskite Tandem Photovoltaic Technologies, *Energy Environ. Sci.*, 2023, **16**, 5551–5567, DOI: **10.1039/D2EE03198A**.

23 V. Larini, C. Ding, F. Faini, G. Pica, G. Bruni, L. Pancini, S. Cavalli, M. Manzi, M. Degani, R. Pallotta, M. De Bastiani, C. Q. Ma and G. Grancini, Sustainable and Circular Management of Perovskite Solar Cells via Green Recycling of Electron Transport Layer-Coated Transparent Conductive Oxide, *Adv. Funct. Mater.*, 2023, 2306040, DOI: **10.1002/adfm.202306040**.

24 C. G. Poll, G. W. Nelson, D. M. Pickup, A. V. Chadwick, D. J. Riley and D. J. Payne, Electrochemical Recycling of Lead from Hybrid Organic-Inorganic Perovskites Using Deep Eutectic Solvents, *Green Chem.*, 2016, **18**(10), 2946–2955, DOI: **10.1039/c5gc02734a**.

25 S. Zhang, L. Shen, M. Huang, Y. Yu, L. Lei, J. Shao, Q. Zhao, Z. Wu, J. Wang and S. Yang, Cyclic Utilization of Lead in Carbon-Based Perovskite Solar Cells, *ACS Sustain. Chem. Eng.*, 2018, **6**(6), 7558–7564, DOI: **10.1021/acssuschemeng.8b00314**.

26 S. Y. Park, J. S. Park, B. J. Kim, H. Lee, A. Walsh, K. Zhu, D. H. Kim and H. S. Jung, Sustainable Lead Management in Halide Perovskite Solar Cells, *Nat. Sustainability*, 2020, **3**(12), 1044–1051, DOI: **10.1038/s41893-020-0586-6**.

27 M. Ren, Y. Miao, T. Zhang, Z. Qin, Y. Chen, N. Wei, X. Qian, T. Wang and Y. Zhao, Lead Stabilization and Iodine Recycling of Lead Halide Perovskite Solar Cells, *ACS Sustain. Chem. Eng.*, 2021, **9**(48), 16519–16525, DOI: 10.1021/acssuschemeng.1c07083.

28 M. Yang, T. Tian, Y. Fang, W. G. Li, G. Liu, W. Feng, M. Xu and W. Q. Wu, Reducing Lead Toxicity of Perovskite Solar Cells with a Built-in Supramolecular Complex, *Nat. Sustainability*, 2023, **6**(11), 1455–1464, DOI: 10.1038/s41893-023-01181-x.

29 F. Schmidt, M. Amrein, S. Hedwig, M. Kober-Czerny, A. Paracchino, V. Holappa, R. Suhonen, A. Schäffer, E. C. Constable, H. J. Snaith and M. Lenz, Organic Solvent Free PbI2 Recycling from Perovskite Solar Cells Using Hot Water, *J. Hazard. Mater.*, 2023, **447**, 130829, DOI: 10.1016/j.jhazmat.2023.130829.

30 F. Meng, J. Bi, J. Chang and G. Wang, Recycling Useful Materials of Perovskite Solar Cells toward Sustainable Development, *Adv. Sustainable Syst.*, 2023, **7**(5), 1–19, DOI: 10.1002/adsu.202300014.

31 B. Chen, C. Fei, S. Chen, H. Gu, X. Xiao and J. Huang, Recycling Lead and Transparent Conductors from Perovskite Solar Modules, *Nat. Commun.*, 2021, **12**(1), 1–10, DOI: 10.1038/s41467-021-26121-1.

32 A. Binek, M. L. Petrus, N. Huber, H. Bristow, Y. Hu, T. Bein and P. Docampo, Recycling Perovskite Solar Cells to Avoid Lead Waste, *ACS Appl. Mater. Interfaces*, 2016, **8**(20), 12881–12886, DOI: 10.1021/acsami.6b03767.

33 B. J. Kim, D. H. Kim, S. L. Kwon, S. Y. Park, Z. Li, K. Zhu and H. S. Jung, Selective Dissolution of Halide Perovskites as a Step towards Recycling Solar Cells, *Nat. Commun.*, 2016, **7**, 1–9, DOI: 10.1038/ncomms11735.

34 European Chemical Agency, Substance infocard- N,N-dimethylformamide, https://echa.europa.eu/it/substance-information/-/substanceinfo/100.000.617.

35 X. Feng, Q. Guo, J. Xiu, Z. Ying, K. W. Ng, L. Huang, S. Wang, H. Pan, Z. Tang and Z. He, Close-Loop Recycling of Perovskite Solar Cells through Dissolution-Recrystallization of Perovskite by Butylamine, *Cell Rep. Phys. Sci.*, 2021, **2**(2), 100341, DOI: 10.1016/j.xcrp.2021.100341.

36 European Chemical Agency, Substance infocard-Butylamine. https://echa.europa.eu/it/substance-information/-/substanceinfo/100.003.364.

37 K. Wang, T. Ye, X. Huang, Y. Hou, J. Yoon, D. Yang, X. Hu, X. Jiang, C. Wu, G. Zhou and S. Priya, "One-Key-Reset" Recycling of Whole Perovskite Solar Cell, *Matter*, 2021, **4**(7), 2522–2541, DOI: 10.1016/j.matt.2021.05.023.

38 P. Shah, S. Parikh, M. Shah and S. Dharaskar, A Holistic Review on Application of Green Solvents and Replacement Study for Conventional Solvents, *Biomass Convers. Biorefin.*, 2022, **12**(5), 1985–1999, DOI: 10.1007/s13399-021-01465-2.

39 D. R. Joshi and N. Adhikari, An Overview on Common Organic Solvents and Their Toxicity, *J. Pharm. Res. Int.*, 2019, **3**(28), 1–18, DOI: 10.9734/jpri/2019/v28i330203.

40 H. S. Kim, Y. J. An, J. Il Kwak, H. J. Kim, H. S. Jung and N. G. Park, Sustainable Green Process for Environmentally Viable Perovskite Solar Cells, *ACS Energy Lett.*, 2022, **7**(3), 1154–1177, DOI: 10.1021/acsenergylett.1c02836.

41 D. Prat, A. Wells, J. Hayler, H. Sneddon, C. R. McElroy, S. Abou-Shehada and P. J. Dunn, CHEM21 Selection Guide of Classical- and Less Classical-Solvents, *Green Chem.*, 2015, **18**(1), 288–296, DOI: 10.1039/c5gc01008j.

42 M. Degani, R. Pallotta, G. Pica, M. Karimipour, A. Mirabelli, K. Frohna, M. Anaya, T. Xu, C. Q. Ma, S. D. Stranks, M. L. Cantù and G. Grancini, Compositional Gradient of Mixed Halide 2D Perovskite Interface Boosts Outdoor Stability of Highly Efficient Perovskite Solar Cells, *Adv. Energy Mater.*, 2025, **15**(17), 2404469, DOI: 10.1002/aenm.202404469.

43 L. Huang, J. Xu, X. Sun, R. Xu, Y. Du, J. Ni, H. Cai, J. Li, Z. Hu and J. Zhang, New Films on Old Substrates: Toward Green and Sustainable Energy Production via Recycling of Functional Components from Degraded Perovskite Solar Cells, *ACS Sustain. Chem. Eng.*, 2017, **5**(4), 3261–3269, DOI: 10.1021/acssuschemeng.6b03089.

44 L. Huang, Z. Hu, J. Xu, X. Sun, Y. Du, J. Ni, H. Cai, J. Li and J. Zhang, Efficient Electron-Transport Layer-Free Planar Perovskite Solar Cells via Recycling the FTO/Glass Substrates from Degraded Devices, *Sol. Energy Mater. Sol. Cells*, 2016, **152**, 118–124, DOI: 10.1016/j.solmat.2016.03.035.

45 L. Pancini, R. Montecucco, V. Larini, A. Benassi, D. Mirani, G. Pica, M. De Bastiani, F. Doria and G. Grancini, A Fluorescent Sensor to Detect Lead Leakage from Perovskite Solar Cells, *Mater, Adv.*, 2023, **4**(11), 2410–2417, DOI: 10.1039/d3ma00068k.

46 R. Frischknecht, G. Heath, M. Raugei, P. Sinha and M. de Wild-Scholten, *Methodology Guidelines on Life Cycle Assessment of Photovoltaic Electricity*, 3rd edn, 2016.

47 S. Manfredi, K. Allacker, N. Pelletier, K. Chomkhamsri and D. M. de Souza, *Product Environmental Footprint (PEF) Guide*, 2012.

48 X. Tian, B. Roose, S. D. Stranks and F. You, Periodic Module Rejuvenation Provides Early Market Entry for Circular All-Perovskite Tandem Photovoltaic Technologies, *Energy Environ. Sci.*, 2023, **16**, 5551–5567, DOI: 10.1039/d2ee03198a.

49 I. Celik, A. B. Phillips, Z. Song, Y. Yan, R. J. Ellingson, M. J. Heben and D. Apul, Environmental Analysis of Perovskites and Other Relevant Solar Cell Technologies in a Tandem Configuration, *Energy Environ. Sci.*, 2017, **10**, 1874–1884, DOI: 10.1039/c7ee01650f.

50 X. Tian, S. D. Stranks and F. You, Life Cycle Energy Use and Environmental Implications of High-Performance Perovskite Tandem Solar Cells, *Sci. Adv.*, 2020, **6**, 1–10.

51 J. Gong, S. B. Darling and F. You, Perovskite Photovoltaics: Life-Cycle Assessment of Energy and Environmental Impacts, *Energy Environ. Sci.*, 2015, **8**, 1953–1968, DOI: 10.1039/c5ee00615e.

52 S. Maranghi, M. L. Parisi, R. Basosi and A. Sinicropi, Environmental Profile of the Manufacturing Process of Perovskite Photovoltaics: Harmonization of Life Cycle Assessment Studies, *Energies*, 2019, **12**(19), 3746, DOI: 10.3390/en12193746.

53 X. Tian, S. D. Stranks and F. You, Life Cycle Assessment of Recycling Strategies for Perovskite Photovoltaic Modules, *Nat. Sustainability*, 2021, **4**(9), 821–829, DOI: 10.1038/s41893-021-00737-z.

54 N. Espinosa, R. García-Valverde, A. Urbina and F. C. Krebs, A Life Cycle Analysis of Polymer Solar Cell Modules Prepared Using Roll-to-Roll Methods under Ambient Conditions, *Sol. Energy Mater. Sol. Cells*, 2011, **95**(5), 1293–1302, DOI: 10.1016/j.solmat.2010.08.020.

55 European Commission, Directive 2008/98/EC of the European Parliament and of the Council of 19 November 2008 on Waste and Repealing Certain Directives, 2018.

56 G. Xing, N. Mathews, S. S. Lim, Y. M. Lam, S. Mhaisalkar and T. C. Sum, Long-Range Balanced Electron- and Hole-Transport Lengths in Organic-Inorganic CH3NH3PbI3, *Science*, 2013, **342**, 344–347.

57 P. Caprioglio, M. Stolterfoht, C. M. Wolff, T. Unold, B. Rech, S. Albrecht and D. Neher, On the Relation between the Open-Circuit Voltage and Quasi-Fermi Level Splitting in Efficient Perovskite Solar Cells, *Adv. Energy Mater.*, 2019, **9**, 1901631.

58 S. Mabrouk, A. Dubey, W. Zhang, B. Bahrami, N. Adhikari, N. Hasan, S. Yang and Q. Qiao, Increased Efficiency for Perovskite Photovoltaics via Doping the PbI2 Layer, *J. Phys. Chem. C*, 2016, **120**, 24577–24582, DOI: 10.1021/acs.jpcc.6b06799.

59 X. Huang, Q. Cui, W. Bi, L. Li, P. Jia, Y. Hou, Y. Hu, Z. Lou and F. Teng, Two-Dimensional Additive Diethylammonium Iodide Promoting Crystal Growth for Efficient and Stable Perovskite Solar Cells, *RSC Adv.*, 2019, **9**, 7984–7991, DOI: 10.1039/C9RA01186B.

60 T. Bu, J. Li, F. Zheng, W. Chen, X. Wen, Z. Ku, Y. Peng, J. Zhong, Y. B. Cheng and F. Huang, Universal Passivation Strategy to Slot-Die Printed SnO2 for Hysteresis-Free Efficient Flexible Perovskite Solar Module, *Nat. Commun.*, 2018, **9**(1), 1–10, DOI: 10.1038/s41467-018-07099-9.

61 M. Abdi-Jalebi, Z. Andaji-Garmaroudi, S. Cacovich, C. Stavrakas, B. Philippe, J. M. Richter, M. Alsari, E. P. Booker, E. M. Hutter, A. J. Pearson, S. Lilliu, T. J. Savenije, H. Rensmo, G. Divitini, C. Ducati, R. H. Friend and S. D. Stranks, Maximizing and Stabilizing Luminescence from Halide Perovskites with Potassium Passivation, *Nature*, 2018, **555**(7697), 497–501, DOI: 10.1038/nature25989.

62 Y. Gao, H. Raza, Z. Zhang, W. Chen and Z. Liu, Rethinking the Role of Excess/Residual Lead Iodide in Perovskite Solar Cells, *Adv. Funct. Mater.*, 2023, 2215171, DOI: 10.1002/adfm.202215171.

63 Q. Chen, H. Zhou, T. B. Song, S. Luo, Z. Hong, H. S. Duan, L. Dou, Y. Liu and Y. Yang, Controllable Self-Induced Passivation of Hybrid Lead Iodide Perovskites toward High Performance Solar Cells, *Nano Lett.*, 2014, **14**(7), 4158–4163, DOI: 10.1021/nl501838y.

64 M. C. Shih, S. S. Li, C. H. Hsieh, Y. C. Wang, H. D. Yang, Y. P. Chiu, C. S. Chang and C. W. Chen, Spatially Resolved Imaging on Photocarrier Generations and Band Alignments at Perovskite/PbI2 Heterointerfaces of Perovskite Solar Cells by Light-Modulated Scanning Tunneling Microscopy, *Nano Lett.*, 2017, **17**(2), 1154–1160, DOI: 10.1021/acs.nanolett.6b04803.

65 J. S. Yun, A. Ho-Baillie, S. Huang, S. H. Woo, Y. Heo, J. Seidel, F. Huang, Y. B. Cheng and M. A. Green, Benefit of Grain Boundaries in Organic-Inorganic Halide Planar Perovskite Solar Cells, *J. Phys. Chem. Lett.*, 2015, **6**(5), 875–880, DOI: 10.1021/acs.jpclett.5b00182.

66 W. Zhang, L. Wang, Y. Guo, B. Zhang, V. Leandri, B. Xu, Z. Li, J. M. Gardner, L. Sun and L. Kloo, Single Crystal Structure and Opto-Electronic Properties of Oxidized Spiro-OMeTAD, *Chem. Commun.*, 2020, **56**(10), 1589–1592, DOI: 10.1039/c9cc09270f.

67 S. Fantacci, F. De Angelis, M. K. Nazeeruddin and M. Grätzel, Electronic and Optical Properties of the Spiro-MeOTAD Hole Conductor in Its Neutral and Oxidized Forms: A DFT/TDDFT Investigation, *J. Phys. Chem. C*, 2011, **115**(46), 23126–23133, DOI: 10.1021/jp207968b.

68 A. Abate, T. Leijtens, S. Pathak, J. Teuscher, R. Avolio, M. E. Errico, J. Kirkpatrik, J. M. Ball, P. Docampo, I. McPherson and H. J. Snaith, Lithium Salts as "Redox Active" p-Type Dopants for Organic Semiconductors and Their Impact in Solid-State Dye-Sensitized Solar Cells, *Phys. Chem. Chem. Phys.*, 2013, **15**(7), 2572–2579, DOI: 10.1039/c2cp44397j.

69 G. Rodriguez-Garcia, E. Aydin, S. De Wolf, B. Carlson, J. Kellar and I. Celik, Life Cycle Assessment of Coated-Glass Recovery from Perovskite Solar Cells, *ACS Sustain. Chem. Eng.*, 2021, **9**(45), 15239–15248, DOI: 10.1021/ACSSUSCHEMENG.1C05029/ASSET/IMAGES/LARGE/SC1C05029_0004.JPEG.